A Computational Investigation of the Multiple Channels of the $NF_2 + F$ Reaction†

Simone S. Ramalho,‡ Patrícia R. P. Barreto,§ João B. L. Martins,|| Geraldo Magela e Silva,⊥ and Ricardo Gargano*,⊥

Instituto Federal de Educação, Ciência e Tecnologia de Goiás, IFG, Av. Universitária, Vale das Goiabeiras, Inhumas, GO, CEP 75400-000, Brazil, Instituto de Física, Universidade de Brasília, CP04455, Brasília, DF, CEP 70919-970, Brazil, LAP, Instituto Nacional de Pesquisas Espaciais, CP515, São José dos Campos, SP, CEP 12247-970, Brazil, and Instituto de Química, Universidade de Brasília, CP4478, 70919-970 Brasília, DF, Brazil

Received: April 7, 2009; Revised Manuscript Received: October 15, 2009

We have theoretically studied the $NF_3 = NF_2 + F$, $NF_2 + F = NF + F_2$, and $NF_2 + F = NF_2 + F$ reactive processes. More precisely, we have evaluated the thermal rate constants (TRC), with the Wigner and Eckart tunneling corrections, minimum energy path, and the intrinsic reaction coordinates of these systems. The $NF_3 = NF_2 + F$ conventional and Wigner TRCs agree very well with experimental data available in the literature for a wide range of temperatures. This study gives a first step to understand and determine the correct decomposition path of nitrogen trifluoride (NF_3).

1. Introduction

Nitrogen trifluoride is useful for plasma or thermal cleaning of chemical vapor deposition reactors. It is also used as a selective reagent for silicon dioxide etching. In the past few years, NF_3 has been preferentially chosen for the reduction of perfluorochemical emission to the environment. Despite of great applicability of NF_3 in many fields of technology,[1−3] the understanding of the chemical processes involved in the mechanism of decomposition of NF_3 is greatly required. Therefore, the most important aim of the research concerned with NF_3 is to investigate its decomposition. In order to understand and determine the correct decomposition path of NF_3 into N_2 and F_2[4] systems, it is important to study several elementary reactions, as an intermediary step, to reach the global reaction.

There are several association, unimolecular ($NF = N + F$, $NF_2 = NF + F$, $NF_3 = NF_2 + F$, $N_2F = N_2 + F$, $N_2F_3 = NF_2 + NF$), abstraction ($NF_2 + F = NF + F_2$, $NF_3 + F = NF_2 + F_2$, $NF + N = N_2 + F$, $NF + F = N + F_2$, $NF_2 + N = NF + NF$, $NF_3 + N = NF_2 + NF$) and exchange ($NF + F = NF + F$, $NF_2 + F = NF_2 + F$, $NF_3 + F = NF_3 + F$) reactions performing a total of 14 reactions that make part of the gas-phase kinetic mechanisms for the N/F/H system.

In this paper, we discuss two possible channels of the reaction involving the NF_2 radical with the fluorine atom: $NF_2 + F = NF + F_2$ (abstraction) and $NF_2 + F = NF_2 + F$ (exchange) channels. Furthermore, we also study the $NF_3 = NF_2 + F$ unimolecular channel. These studies have been done using conventional transition state theory (TST) and also including two different corrections (Wigner[5] and Eckart[6]) for the tunneling effects.

The paper is organized as follows. In section 2 we present the main features of our code. Section 3 outlines the computational details. Our results and discussion are presented in section 4. The conclusions are presented in section 5.

2. Thermal Rate Constant Calculation

The TRC of a bimolecular reaction, $A + BC \rightarrow X^{\ddagger} \rightarrow C + AB$, via TST theory, can be written as[5,7−10]

$$k^{\mathrm{TST}} = \frac{k_B T}{h} \frac{Q_{X^{\ddagger}}}{Q_A Q_{BC}} \exp\left(-\frac{V_a^{\mathrm{G}}}{RT}\right) \tag{1}$$

where $Q_{X^{\ddagger}}$, Q_A, and Q_{BC} are the partition functions of transition state (TS) and reactants ($A + BC$), respectively. k_B is Boltzmann's constant, h is Planck's constant, T is the temperature, R is the gas constant, and V_a^G is the potential barrier

$$V_a^G = V_{\mathrm{MEP}} + \varepsilon_{\mathrm{ZPE}} \tag{2}$$

where $\varepsilon_{\mathrm{ZPE}}$ is the harmonic zero-point energies (ZPE) and V_{MEP} is the Eckart classical potential energy[6] measured from the overall zero energy of the reactants

$$V_{\mathrm{MEP}} = \frac{ay}{1+y} + \frac{by}{(1+y)^2} \tag{3}$$

where

$$y = e^{\alpha(s-s_0)} \tag{4}$$

† Part of the "Vincenzo Aquilanti Festschrift".

* Corresponding author: tel, +55(61) 3307-2900; fax, +55(61) 3307-2363; e-mail, gargano@fis.unb.br (Ricardo Gargano).
‡ Instituto Federal de Educação, Ciência e Tecnologia de Goiás, IFG.
§ LAP, Instituto Nacional de Pesquisas Espaciais.
|| Instituto de Química, Universidade de Brasília.
⊥ Instituto de Física, Universidade de Brasília.

10.1021/jp903221b
Published on Web 11/04/2009

$$a = \Delta H_0^0 = V_a^{G^\ddagger}(s = +\text{inf}) - V_a^{G^\ddagger}(s = -\text{inf}) \quad (5)$$

$$b = (2V_a^{G^\ddagger} - a) + 2(V_a^{G^\ddagger}(V_a^{G^\ddagger} - a))^{1/2} \quad (6)$$

$$s_0 = -\frac{1}{\alpha}\ln\left(\frac{a+b}{b-a}\right) \quad (7)$$

$$\alpha^2 = -\frac{\mu(\omega^\ddagger)^2 b}{2V^\ddagger(V^\ddagger - a)} \quad (8)$$

here μ is the reduced mass. a and b depend on the reactants ($V_a^{G^\ddagger}(s = -\text{inf})$), products ($V_a^{G^\ddagger}(s = +\text{inf})$), and TS ($V_a^{G^\ddagger}$) energies, as well as the imaginary frequency on the TS ($\omega^\ddagger$),[11,12] and y is related to the reaction coordinate.

Introducing the transmission coefficient, $\kappa_{W/E}(T)$, eq 1 becomes

$$k = \kappa_{W/E}(T)k^{TST}(T) \quad (9)$$

where $\kappa_{W/E}(T)$ is used to account for the tunneling effect (using Wigner or Eckart correction) along the reaction coordinate. The Wigner correction ($\kappa_W(T)$) for tunneling assumes a parabolic potential for the nuclear motion near to TS, and therefore the values are underestimated. The Wigner transmission coefficient is given by[5,13]

$$\kappa_W(T) = 1 + \frac{1}{24}\left|\frac{\hbar\omega^\ddagger}{k_B T}\right|^2 \quad (10)$$

The Eckart tunneling correction ($\kappa_E(T)$) is obtained solving the Schrödinger equation for the V_{MEP}. This yields the transmission probability ($\Gamma(E)$) given by[6,12,14]

$$\Gamma(E) = 1 - \frac{\cosh[2\pi(\delta - \beta)] + \cosh[2\pi\gamma]}{\cosh[2\pi(\delta + \beta)] + \cosh[2\pi\gamma]} \quad (11)$$

where

$$\delta = \frac{1}{2}\left(\frac{E}{c}\right)^{1/2} \quad (12)$$

$$\beta = \frac{1}{2}\left(\frac{E-a}{c}\right)^{1/2} \quad (13)$$

$$\gamma = \frac{1}{2}\left(\frac{b-c}{c}\right)^{1/2} \quad (14)$$

$$c = \frac{(h\omega^\ddagger)^2 b}{16\Delta V^\ddagger(\Delta V^\ddagger - a)} \quad (15)$$

where $\Delta V^\ddagger$ is the zero point energy corrected barrier at TS relative to reactants (the parameters a and b were defined above).

The $\kappa_E(T)$ is obtained as the ratio between the quantum mechanical and the classical thermal rate constants, which is calculated by integrating the respective transmission probabilities over the entire energies range

$$\kappa_E(T) = \frac{\exp(\Delta V^\ddagger/RT)}{RT}\int_0^\infty \exp(-E/RT)\Gamma(E)\,dE \quad (16)$$

For higher accuracy, the variational transition state theory should be used and also the semiclassical methods for the tunneling effect.[5] The characteristics of the MEP and the TRC, with the Wigner and Eckart tunneling corrections, were determined using our own code, which is described in the literature.[8−10] The TRCs were then written in the Arrhenius form as

$$k(T) = AT^N \exp\left(-\frac{E_a}{RT}\right) \quad (17)$$

where A is the pre-exponential factor, N is the temperature power factor, and E_a is the activation energy.

3. Computational Details

To apply TST theory, we must know the geometries, frequencies, and the potential energy for the reactants, products and TS of the $NF_3 = NF_2 + F$, $NF_2 + F = NF + F_2$, and $NF_2 + F = NF_2 + F$ reactions. These properties were obtained from accurate electronic structure calculations performed using the GAUSSIAN03 program.[15] The TS of these reactions were determined using the full (all electrons included in the correlation calculation) second-order Møller−Plesset (MP2) level of theory with the 6-31G(d) and cc-pVDZ basis sets. The methodology used for this study was employed with aceptable accordance compared to the theoretical and experimental data for different systems.[8−10]

We have also used extended basis sets at higher levels of theory in order to increase the accuracy of calculated data. Therefore, two sets of energies were determined for these reactions. Starting from MP2/cc-pVDZ optimized geometries, the first set was determined using the aug-cc-pVDZ, cc-pVTZ, and aug-cc-pVTZ Dunning basis sets at MP4(SDQ), MP4(SDTQ), QCISD, QCISD(T), CCSD, and CCSD(T) levels. The second set was determined starting from MP2/6-31G(d) optimized geometries at the same six levels of calculations and the following Pople basis sets: 6-31++G(d,p), 6-311++G(d,p), 6-311++G(df,pd), and 6-311++G(3df,3pd). We had also reoptimized the geometries using the MP2/aug-cc-pVTZ level in order to study the basis set superposition error and increase the accuracy of the calculated TRC values. The properties of these systems are compared to the experimental data available.[16−19] The frequencies related to each reaction were scaled by the factors 0.977884 and 0.962846 for the cc-pVDZ and 6-31G(d) basis sets, respectively. The scale factor was calculated using the following expression

$$\text{scale factor} = \frac{\sum_{i=1}^{N} w_i(\text{exptl})/w_i(\text{theor})}{N} \quad (18)$$

where N is the number of frequencies and w_i(exptl) and w_i(theor) are the experimental and theoretical vibrational frequencies.

4. Results and Discussion

Table 1 shows the equilibrium geometries for the reactants and products calculated at the full MP2 level with the cc-pVDZ, 6-31G(d) and aug-cc-pVTZ basis sets, for all species involved

TABLE 1: Geometrical Parameters for Reactants and Products of the Unimolecular, Abstraction and Exchange Reactions Calculated at MP2/cc-pVDZ, MP2/6-31G(d), and MP2/aug-cc-pVTZ Levels

		interatomic distances (Å)		bond angles (deg)
species	bases	R_{NF}	R_{FF}	A_{FNF}
F_2	cc-pVDZ		1.424	
	6-31G(d)		1.421	
	aug-cc-pVTZ		1.398	
	exptl		1.412[20]	
			1.412[22]	
			1.435[23]	
	theor		1.421[24]	
NF	cc-pVDZ	1.317		
	6-31G(d)	1.330		
	aug-cc-pVTZ	1.290		
	exptl	1.317[21]		
		1.317[22]		
		1.510[20]		
	theor	1.330[24]		
NF_2	cc-pVDZ	1.349		103.7
	6-31G(d)	1.359		103.3
	aug-cc-pVTZ	1.340		103.4
	exptl	1.370[20,25]		104.2[20,25]
	theor	1.359[24]		103.3[24]
NF_3	cc-pVDZ	1.377		102.0
	6-31G(d)	1.385		101.7
	aug-cc-pVTZ	1.364		101.8
	exptl	1.371[20]		102.9[20]
	theor	1.385[26]		101.7[26]
		1.380[24]		101.7[24]

in these reactions, and compares these values with experimental and theoretical reference data.[20−27] The interatomic distance and bond angle absolute errors for all species are smaller than 0.220 Å and 1.2°, respectively, when compared to the experimental data.[20−23,25−27] The absolute errors are 0.040 Å and 0.4° when compared to the theoretical data using G2, G3, and B3LYP/6-311++G(3df,3pd) level of theory,[24] respectively.

The calculated frequency values (Table 2) show no significant average errors compared with the experimental data. The frequencies give the ZPE used to obtain the barrier in the eq 2. The frequencies related to each reaction were scaled (see Computational Details). This is done to take into account known deficiencies at the MP2 level for the basis sets used. The aug-cc-pVTZ basis set shows vibrational frequency values slightly larger than the experimental data. The unimolecular, abstraction, and exchange ZPE were also scaled by the same factors.

Table 3 shows the TS optimized geometry and harmonic frequencies, at the full MP2 level of theory with the cc-pVDZ and 6-31G(d) basis sets, for unimolecular (TS_1), abstraction (TS_2), and exchange (TS_3) reactions, respectively. For the unimolecular reaction, the aug-cc-pVTZ results are also shown. Structures a, b, and c of Figure 1 show a schematic representation of the TS_1, TS_2, and TS_3 transition structures geometries at MP2/cc-pVDZ level, respectively. They provide also the notation used in Table 3. The optimized NF distance (R_{NF}) of the TS structures show a small deviation from the experimental data found for the NF_3 gas phase molecule (1.365 Å).[16]

Table 4 shows the reactant and product formation enthalpy with ZPE correction for all species involved in unimolecular, abstraction, and exchange reactions and compares also these values with both theoretical and experimental data available in the literature. The calculated results are in a good agreement with theoretical and experimental ones.

The ZPE correction for the evaluation of ΔE (or ΔH) for the reaction, $ZPE_{corr} = \varepsilon_{ZPE_{prod}} - \varepsilon_{ZPE_{react}}$, were determined in order

TABLE 2: Harmonic Vibrational Frequencies (cm^{-1}) and Zero-Point Energy (kcal mol^{-1}) for Reactants and Products of the Unimolecular, Abstraction, and Exchange Reactions at MP2/cc-pVDZ, MP2/6-31G(d), and MP2/aug-cc-pVTZ Levels

species	bases	ν_1	ν_2	ν_3	ν_4	ε_{ZPE}
F_2	cc-pVDZ	933.4				1.3
	6-31G(d)	1007.8				1.4
	aug-cc-pVTZ	1009.4				1.4
	exptl	892.0[23,27]				
		916.6[22]				
	theor	957.0[24]				
NF	cc-pVDZ	1175.3				1.6
	6-31G(d)	1192.0				1.6
	aug-cc-pVTZ	1251.9				1.8
	exptl	1115.0[20]				
		1141.4[21,22]				
	theor	1138.5[21]				
		1104.6[24]				
NF_2	cc-pVDZ	586.0	982.8	1126.6		3.8
	6-31G(d)	574.0	1026.1	1147.0		3.9
	aug-cc-pVTZ	596.0	979.3	1133.7		3.9
	exptl	573.0[20]	931.0[20]	1074.0[20]		
		573.4[25]	930.7[25]	1069.5[25]		
	theor	569.7[24]	908.1[24]	1078.6[24]		
NF_3	cc-pVDZ	496.8	656.1	915.8	1043.8	6.3
	6-31G(d)	489.3	653.7	959.9	1062.0	6.4
	aug-ccpVTZ	511.16	674.6	930.1	1066.0	6.6
	exptl	492.0[20]	642.0[20]	906.0[20]	1032.0[20]	
		497.0[28]	648.0[28]	898.0[28]	1027.0[28]	
	theor	489.3[26]	653.7[26]	959.3[26]	1061.6[26]	
		484.6[24]	644.2[24]	860.6[24]	1032.8[24]	

to take into account that the minimum of the potential energy curve is not the minimum energy of the vibrational ground state ($\nu = 0$). The Supporting Information shows the ab initio total electronic energies, forward barrier ($V_f + ZPE_{corr}$), reverse barrier ($V_r + ZPE_{corr}$), calculated ΔH^0 at 298 K (ΔH^0 at $0K + ZPE_{corr}$), and experimental $\Delta_f H^0$. These properties were determined using the cc-pVDZ, aug-cc-pVDZ, cc-pVTZ, and aug-cc-pVTZ Dunning basis sets and also 6-31G(d), 6-31++G(d,p), 6-311++G(d,p), 6-311++G(df,pd), and 6-311++G(3df,3pd) Pople basis sets at the MP2, MP4(SDQ), MP4(SDTQ), QCISD, QCISD (T), CCSD, and CCSD(T) levels of theory for reactant, product, and TS for the unimolecular, abstraction, and exchange reactions. From an analysis of these results a minor difference between ab initio and experimental $\Delta_f H°$ for the unimolecular, abstraction, and exchange reactions was found with cc-pVTZ basis set at MP4 level. Then for these reactions the TRC were calculated using the MP4/cc-pVTZ level.

The TRC for the unimolecular, abstraction and exchange channels are shown in Figures 2, 3, and 4, respectively. They were evaluated considering conventional TST and also applying the transmission coefficient of Wigner and Eckart in the temperature range of 200−4000 K. One can see from these figures that the tunneling effects are not very important, especially for the exchange channel. This fact was expected, since the skew angle[5] value for this reaction is 68.57°, which is considered as an intermediate value. It indicates that the tunneling effects are not critical for this reaction. These figures show that the unimolecular TRC with the Eckart tunneling correction (Figure 2) is faster than abstraction (Figure 3) and exchange (Figure 4) ones, respectively.

Tables 5 and 6 show a comparison among theoretical and experimental TRC values for a range of available experimental temperatures, using optimized geometries at MP2/cc-pVDZ (Table 5) and MP2/aug-cc-pVTZ (Table 6) levels. The calculated data from the optimized MP2/cc-pVDZ geometry shows TRC values larger than the experimental data, while the data from the MP2/aug-cc-pVTZ geometries are smaller than the experimental data.

TABLE 3: Transition State Geometrical Parameters (interatomic distances in Å and bond angles in degrees), Harmonic Vibrational Frequencies (cm^{-1}), and Zero-Point Energy (kcal mol^{-1}) Calculated at MP2/cc-pVDZ, MP2/6-31G(d), and MP2/aug-cc-pVTZ Levels for the Unimolecular (TS_1), Abstraction (TS_2), and Exchange (TS_3) Reactions[a]

	$NF_3 = NF_2 + F$ (TS_1)			$NF_2 + F = NF + F_2$ (TS_2)		$NF_2 + F = NF_2 + F$ (TS_3)	
	cc-pVDZ	6-31G(d)	aug-cc-pVTZ	cc-pVDZ	6-31G(d)	cc-pVDZ	6-31G(d)
R_{NF}	1.373	1.384	1.401	1.291	1.316	1.311	1.336
$R_{NF'}$	2.593	2.740	2.897	1.913	1.770	1.639	1.703
$R_{NF''}$						1.614	1.538
R_{FF}				1.514	1.518		
$A_{FNF'}$	102.0	102.0	100.9	104.5	103.9	96.4	96.8
$A_{F'NF''}$	106.2	106.3	11.6			167.0	168.3
$A_{NF'F''}$				151.1	136.7		
ν_1	97.4	93.7	95.1	89.2	90.7	307.3	318.6
ν_2	181.1	174.3	192.0	192.9	223.5	559.4	549.6
ν_3	555.8	548.7	529.4	335.7	335.8	593.8	620.9
ν_4	892.9	943.2	880.1	500.8	618.2	1089.7	1100.8
ν_5	1080.2	1104.1	1068.7	1253.5	1196.4	4446.4	5154.3
ν_i	331.3i	335.6i	271.2i	762.1i	794.7i	283.2i	422.2i
ε_{ZPE}	3.9	3.9	3.9	3.3	3.4	9.8	10.7

[a] The imaginary frequency (ν_i) is also reported.

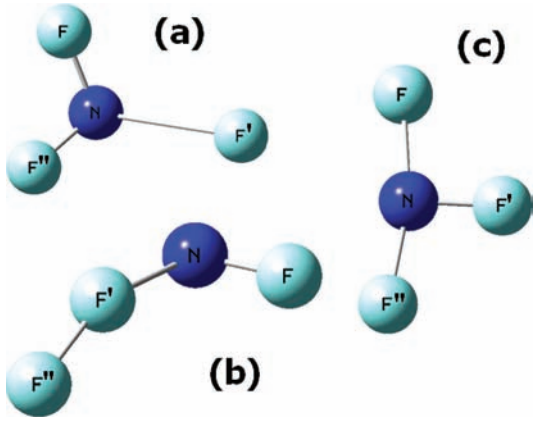

Figure 1. Schematic representation of transition structures for (a) unimolecular (TS_1), (b) abstraction (TS_2), and (c) exchange (TS_3) reactions.

TABLE 4: Reactant and Product Formation Enthalpy (kcal mol^{-1}) with ZPE Correction for All Species Involved in the Unimolecular, Abstraction, and Exchange Reactions

species	this work	experimental references	theoretical references
F		18.47 ± 0.07,[20] 18.46 ± 0.07,[29] 18.92[27]	
F_2	0.403	0	0.3[a], 0.3[b], 0.688[i], 1.288[j] 0.980[c], 0.056[d], 0.686[e] −2.027[c], 0.927[d], −2.142[e]
NF	53.757	55.688 ± 0.72,[29] 55.6 ± 0.5,[30] 59.501 ± 7.89[20]	54.9[a], 54[f], 53.9[g], 56.18[h] 46.698[c], 54.635[d], 51.903[e]
NF_2	7.234	10.7 ± 1.91,[20] 8.8 ± 1.20,[29] 8 ± 1,[27] 8.3 ± 0.5[30]	6.6[a], 8[f], 8.5[g], 8.67[h] −3.411[c], 5.845[d], 5.852[e]
NF_3	−31.600	−30.20 ± 0.27[20,29]	−33.8[b], −26.5[g], −30.2[f] −41.310[c], −35.271[d], −32.321[e]

[a] At G2 level.[31] [b] at G2 level.[32] [c] at B3LYP/6-311++(3df,3pd) level.[24] [d] at G2 level.[24] [e] at G3 level.[24] [f] For G3 level.[33] [g] at BAC-MP4(SDTQ) level.[34] [h] at CCSD(T) level.[35] [i] estimated from $\Delta_f H^0(298)$ at G3 level.[36,37] [j] Estimated from $\Delta_f H^0(298)$ at G3 level.[36,37]

The unimolecular conventional and Wigner TRC agree very well with experimental data of Diesen[17] at 1800 K (Table 5). For the temperature ranges of 1330−2000 K and 1150−1390 K, these results are in a excellent accordance with experimental data of Bird et al.[18] and MacFadden et al.,[19] respectively.

Figure 5 shows the V_{MEP} and V_a^G plots along the MEP, as a function of the reaction coordinates, for the unimolecular reaction. The same plots for the abstraction and exchange reactions are shown in Figures 6 and 7, respectively. In the case of the unimolecular reaction (Figure 5), from $-\infty$ to $-8\ \mu^{1/2}a_o$, the potential curve changes slowly, and it increases gradually after $-8\ \mu^{1/2}a_o$ and decreases quickly after passing the transition state (an endothermic reaction). The same behavior was found for the abstraction reaction (Figure 6). The exchange reaction potential curve (Figure 7) changes slowly from $-\infty$ to $-12.5\ \mu^{1/2}a_0$ and it increases gradually after $-12.5\ \mu^{1/2}a_0$, while it decreases quickly after passing the transition state.

To complete this study, we have also determined the intrinsic reaction coordinates (IRC) for unimolecular, abstraction, and exchange reactions. They are shown in Figures 8, 9, and 10, respectively. From Figure 8, one can verify that the internuclear distance of NF″ increases, while the NF and NF′ internuclear distances remain unchanged. This fact shows the dissociation of the NF_3 molecule and the formation of NF_2 molecule (unimolecular reaction). Figure 9 shows an increase of the NF′ internuclear distance, i.e., the break of NF′ internuclear distance of NF_2 molecule, while the F′F″ decreases, yielding the F_2 molecule (abstraction reaction). Finally, from Figure 10, one can note that the NF′ internuclear distance increases while the NF″ internuclear distance decreases. This feature shows an exchange between the F atoms of the NF_2 + F = NF_2 + F reaction. Figures 9 and 10 show clearly that the fluorine atom of the NF_2 radical is transferred to abstraction and exchange channels.

Arrhenius coefficients were determined from the fitting of TRC obtained through TST theory. The temperature dependence of the overall unimolecular Arrhenius TRC ($cm^3\ mol^{-1}\ s^{-1}$) for the cc-pVDZ basis set can be described by the expression $k = 5.244 \times 10^{17}T^{0.3067} \exp(-6311/RT)$, for conventional TST. Arrhenius form considering the Wigner and Eckart tunneling corrections can be described by $k = 4.137 \times 10^{17}T^{0.3341} \exp(-6300/RT)$ and $k = 3.945 \times 10^{17}T^{0.3397} \exp(-1136/RT)$, respectively. For the aug-cc-pVTZ basis set the temperature dependence of the overall unimolecular Arrhenius TRC can be described by the expressions $k = 2.264 \times 10^{17}T^{0.3450} \exp(-7796/RT)$, $k = 1.918 \times 10^{17}T^{0.3641} \exp(-7789/RT)$, and $k = 1.939 \times$

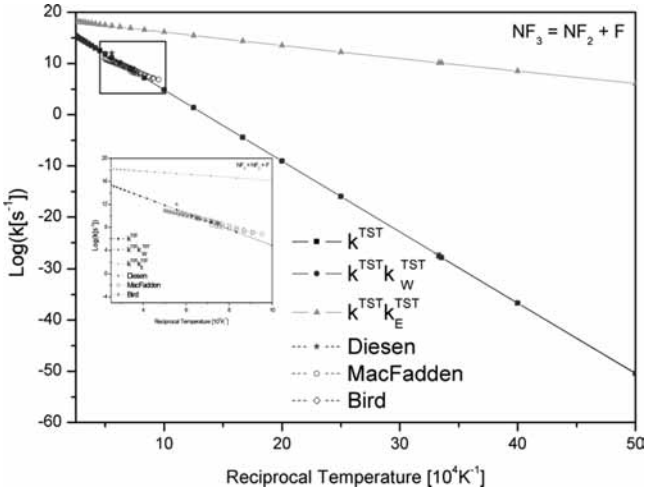

Figure 2. Conventional, Wigner, and Eckart plots of thermal rate constants against the reciprocal temperature in the range of 200−4000 K for the $NF_3 = NF_2 + F$ unimolecular reaction.

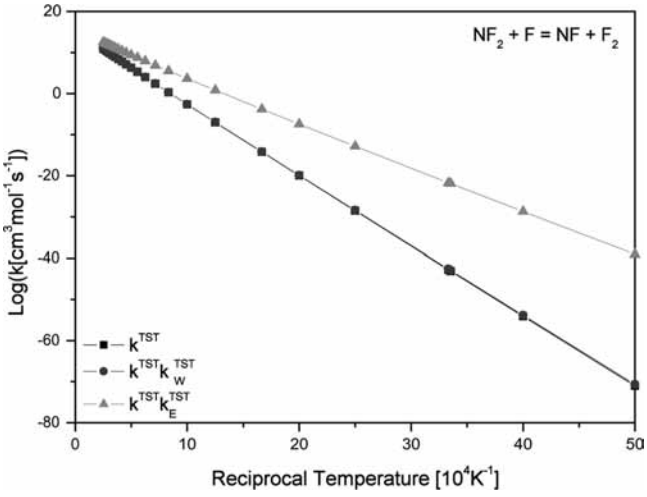

Figure 3. Conventional, Wigner, and Eckart plots of thermal rate constants against the reciprocal temperature in the range of 200−4000 K for the $NF_2 + F = NF + F_2$ abstraction reaction.

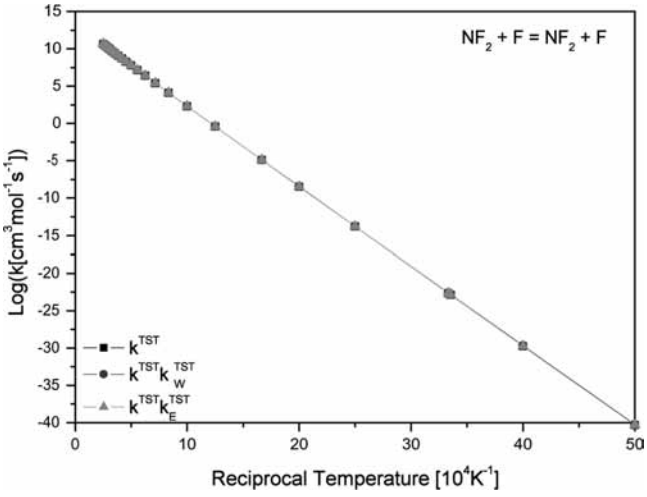

Figure 4. Conventional, Wigner, and Eckart plots of thermal rate constants against the reciprocal temperature in the range of 200−4000 K for the $NF_2 + F = NF_2 + F$ exchange reaction.

$10^{17}T^{0.3625}\exp(-1228/RT)$, for conventional, Wigner, and Eckart, respectively. For the abstraction reactions the Arrhenius expressions are given by $k = 1.9579 \times 10^{9}T^{1.6328}\exp(-76999/RT)$, $k = 8.7971 \times 10^{8}T^{1.7241}\exp(-76565/RT)$, and $k = 2.1604 \times 10^{8}T^{1.8898}\exp(-47568/RT)$, for the conventional, Wigner, and Eckart correction, respectively. The expressions for the Arrhenius exchange reactions were $k = 2.3993 \times 10^{10}T^{0.80246}\exp(-48082/RT)$ and $k = 2.0053 \times 10^{10}T^{0.82318}\exp(-47998/RT)$, for conventional and Wigner, respectively. The Eckart Arrhenius expression for this exchange reaction was overestimated, and it is not shown. In general, the Eckart Arrhenius TRC gives much higher rate constants compared to conventional and Wigner due to its one-dimensional potential barrier.[6] For higher accuracy variational transition state theory should be used

TABLE 5: Calculated Thermal Rate Constants (s^{-1}) Compared to the Experimental Data for $NF_3 = NF_2 + F$ Reaction, Using Optimized Geometries at MP2/cc-pVDZ Level

temp (K)	conventional	Wigner	Eckart	exptl[18]	exptl[19]
1150	6.6747	6.6778	16.4894		7.3809
1200	7.1816	7.1844	16.5873		7.6192
1250	7.6480	7.6507	16.6774		7.8385
1300	8.0787	8.0811	16.7607		8.0409
1330	8.3216	8.3239	16.8077	8.6695	8.1550
1350	8.4776	8.4798	16.8379	8.7687	8.2282
1390	8.7760	8.7782	16.8957	8.9585	8.3685
1400	8.8480	8.8501	16.9097	9.0042	
1450	9.1930	9.1949	16.9766	9.2235	
1500	9.5150	9.5168	17.0391	9.4282	
1530	9.6981	9.6998	17.0746	9.5446	
1550	9.8162	9.8180	17.0976	9.6200	
1600	10.0987	10.1003	17.1525	9.7992	
1650	10.3642	10.3657	17.2041	9.9678	
1700	10.6140	10.6154	17.2527	10.1265	
1750	10.8496	10.8509	17.2986	10.2761	
1800[a]	11.0721	11.0734	17.3419	10.4174	
1850	11.2826	11.2838	17.3830	10.5511	
1900	11.4821	11.4832	17.4219	10.6778	
1950	11.6713	11.6724	17.4588	10.7979	
2000	11.8511	11.8522	17.4939	10.9120	

[a] Experimental thermal rate constant from Diesen et al.[17] value of 12.0 s^{-1} at 1800 K.

TABLE 6: Calculated Thermal Rate Constants (s^{-1}) Compared to the Experimental Data for $NF_3 = NF_2 + F$ Reaction, Using Optimized Geometries at MP2/aug-cc-pVTZ Level

temp (K)	conventional	Wigner	Eckart	exptl[18]	exptl[19]
1150	3.6055	3.6076	16.0748		7.3809
1200	4.2309	4.2328	16.1806		7.6192
1250	4.8064	4.8081	16.2780		7.8385
1300	5.3377	5.3393	16.3680		8.0409
1330	5.6374	5.6389	16.4189	8.6695	8.1550
1350	5.8298	5.8313	16.4515	8.7687	8.2282
1390	6.1980	6.1994	16.5141	8.9585	8.3685
1400	6.2868	6.2882	16.5291	9.0042	
1450	6.7123	6.7137	16.6015	9.2235	
1500	7.1096	7.1108	16.6690	9.4282	
1530	7.3355	7.3367	16.7075	9.5446	
1550	7.4813	7.4824	16.7323	9.6200	
1600	7.8298	7.8309	16.7917	9.7992	
1650	8.1572	8.1582	16.8475	9.9678	
1700	8.4654	8.4664	16.9001	10.1265	
1750	8.7560	8.7569	16.9497	10.2761	
1800[a]	9.0306	9.0314	16.9966	10.4174	
1850	9.2902	9.2910	17.0410	10.5511	
1900	9.5363	9.5371	17.0830	10.6778	
1950	9.7697	9.7705	17.1229	10.7979	
2000	9.9916	9.9922	17.1609	10.9120	

[a] Experimental thermal rate constant from Diesen et al.[17] value of 12.0 s^{-1} at 1800 K.

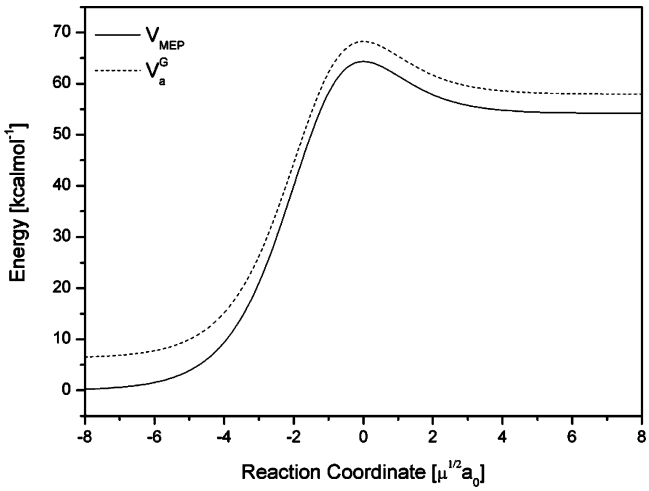

Figure 5. V_{MEP} and V_a^G as function of reaction coordinate for the $NF_3 = NF_2 + F$ unimolecular reaction.

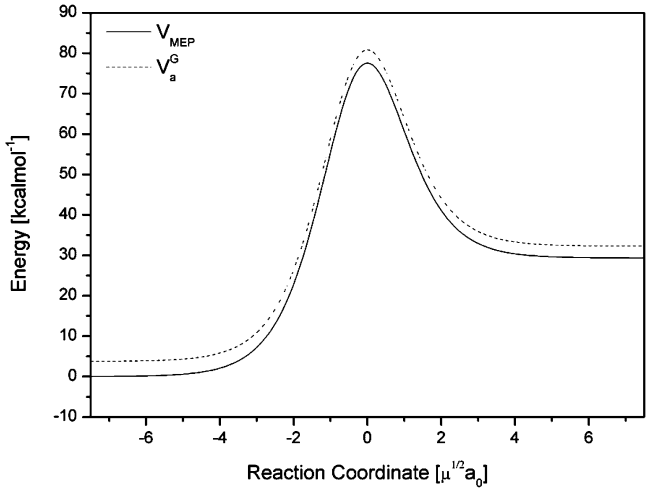

Figure 6. V_{MEP} and V_a^G as function of reaction coordinate for the $NF_2 + F = NF + F_2$ abstraction reaction.

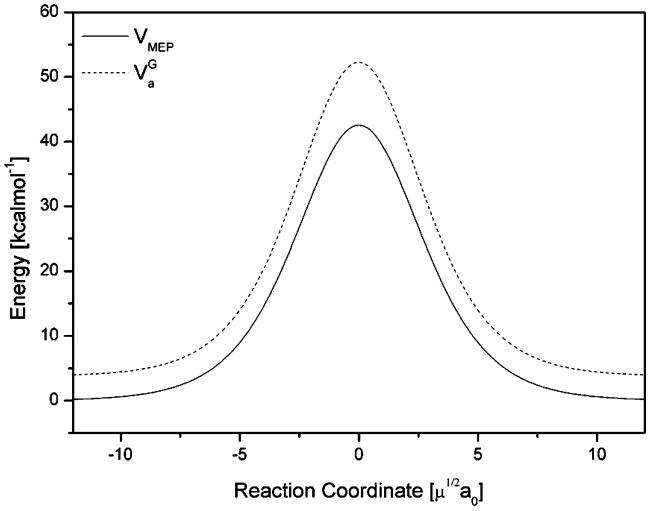

Figure 7. V_{MEP} and V_a^G as function of reaction coordinate for the $NF_2 + F = NF_2 + F$ exchange reaction.

and also semiclassical methods for the tunneling effect,[38] but the required additional information about the potential energy surface was not obtained in the present Letter. The results of the abstraction and exchange reactions using aug-cc-pVTZ optimized geometry are not significantly different from cc-pVDZ data.

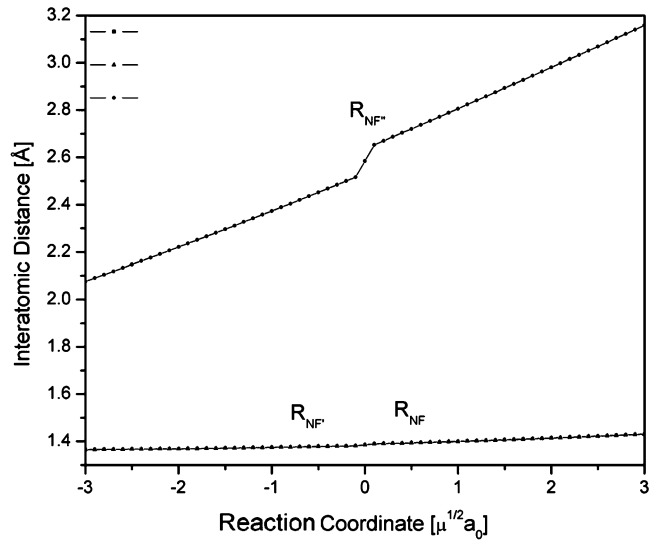

Figure 8. IRC for the $NF_3 = NF_2 + F$ unimolecular reaction.

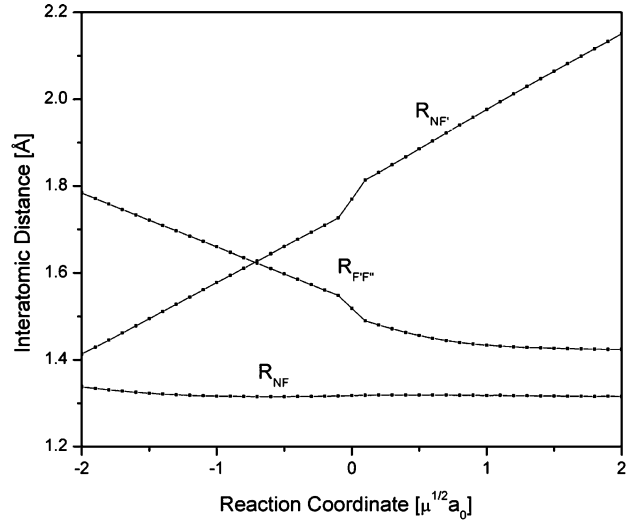

Figure 9. IRC for the $NF_2 + F = NF + F_2$ abstraction reaction.

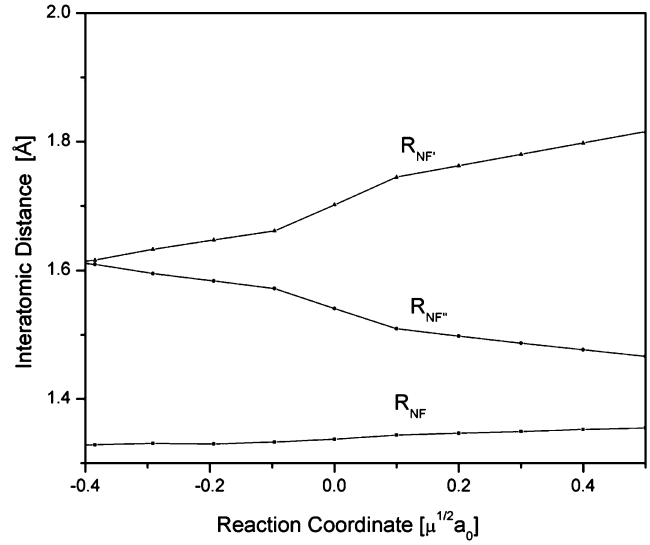

Figure 10. IRC for the $NF_2 + F = NF_2 + F$ exchange reaction.

5. Conclusions

In this paper an accurate ab initio study was done for the $NF_3 = NF_2 + F$, $NF_2 + F = NF + F_2$ and $NF_2 + F = NF_2 +$

F reactions. This study is a first step in the understanding of the correct decomposition path of nitrogen trifluoride. The best enthalpy of the unimolecular, abstraction, and exchange reactions were found at MP4/cc-pVTZ level. The calculated $NF_3 = NF_2 + F$ conventional and Wigner TRCs are in a good agreement with experimental data available in the literature.

Acknowledgment. This paper is dedicated to Professor Vincenzo Aquilanti, with thanks for helpful discussions on topics pertinent to this work. The authors are grateful to the CENAPAD-SP for the provision of computational facilities and also to FINATEC and CNPq for financial support.

Supporting Information Available: Ab initio total electronic energies, forward barrier, reverse barrier, calculated ΔH^0 at 298 K, and experimental $\Delta_f H^0$. This material is available free of charge via the Internet at http://pubs.acs.org.

References and Notes

(1) Shaw, M. J.; Jones, J. D. C. *Appl. Phys.* **1977**, *14*, 393.
(2) Antoniotti, P.; Grandinetti, F. *Chem. Phys. Lett.* **2002**, *366*, 676.
(3) Donnelly, V. M.; Flamm, D. L.; Dautremont-Smith, W. C.; Werder, D. J. *J. Appl. Phys.* **1984**, *55*, 242.
(4) Wang, J. J.; Lambers, E. S.; Pearton, S. J.; Ostling, M.; Zetterling, C. M.; Grow, J. M.; Ren, F. *Solid-State Electron.* **1998**, *42*, 743.
(5) Truhlar, D. G.; Isaacson, A. D.; Garrett, B. C. In *Theory of Chemical Reaction Dynamics*; Baer, M. C., Ed.; CRC Press: Boca Raton, FL, 1985; Vol. 2.
(6) Eckart, C. *Phys. Rev.* **1930**, *35*, 1303.
(7) Pilling, M. J.; Seakings, P. W. *Reaction Kinetic*, 2nd ed.; Oxford Science: Oxford, U.K.; 1995; Vol. 4.
(8) Barreto, P. R. P.; Vilela, A. F. A.; Gargano, R. *J. Mol. Struct.: THEOCHEM* **2003**, *639*, 167.
(9) Barreto, P. R. P.; Vilela, A. F. A.; Gargano, R. *Int. J. Quantum Chem.* **2005**, *103*, 685.
(10) Ramalho, S. S.; Barreto, P. R. P.; Vilela, A. F. A.; Gargano, R. *Chem. Phys. Lett.* **2005**, *413*, 151.
(11) Truong, T. N.; Truhlar, D. G. *J. Chem. Phys.* **1990**, *93*, 1761.
(12) Pardo, L.; Banfelder, J. R.; Osman, R. *J. Am. Chem. Soc.* **1992**, *114*, 2382.
(13) Henon, E.; Bohr, F. *J. Mol. Struct.: THEOCHEM* **2000**, *531*, 283.
(14) Johnston, H. S.; Heicklen, J. *J. Phys. Chem.* **1962**, *66*, 532.
(15) Frisch, M. J.; Trucks, G. W.; Schlegel, H. B.; Scuseria, G. E.; Robb, M. A.; Cheeseman, J. R.; Montgomery, J. A., Jr.; Vreven, T.; Kudin, K. N.; Burant, J. C.; Millam, J. M.; Iyengar, S. S.; Tomasi, J.; Barone, V.; Mennucci, B.; Cossi, M.; Scalmani, G.; Rega, N.; Petersson, G. A.; Nakatsuji, H.; Hada, M.; Ehara, M.; Toyota, K.; Fukuda, R.; Hasegawa, J.; Ishida, M.; Nakajima, T.; Honda, Y.; Kitao, O.; Nakai, H.; Klene, M.; Li, X.; Knox, J. E.; Hratchian, H. P.; Cross, J. B.; Bakken, V.; Adamo, C.; Jaramillo, J.; Gomperts, R.; Stratmann, R. E.; Yazyev, O.; Austin, A. J.; Cammi, R.; Pomelli, C.; Ochterski, J. W.; Ayala, P. Y.; Morokuma, K.; Voth, G. A.; Salvador, P.; Dannenberg, J. J.; Zakrzewski, V. G.; Dapprich, S.; Daniels, A. D.; Strain, M. C.; Farkas, O.; Malick, D. K.; Rabuck, A. D.; Raghavachari, K.; Foresman, J. B.; Ortiz, J. V.; Cui, Q.; Baboul, A. G.; Clifford, S.; Cioslowski, J.; Stefanov, B. B.; Liu, G.; Liashenko, A.; Piskorz, P.; Komaromi, I.; Martin, R. L.; Fox, D. J.; Keith, T.; Al-Laham, M. A.; Peng, C. Y.; Nanayakkara, A.; Challacombe, M.; Gill, P. M. W.; Johnson, B.; Chen, W.; Wong, M. W.; Gonzalez, C.; Pople, J. A. *Gaussian 03, Revision E.01*; Gaussian, Inc.: Wallingford, CT, 2004.
(16) Kuchitsu, K. *Structure of Free Polyatomic Molecules - Basic Data*; Springer: Berlin; 1998.
(17) Diesen, R. W. *J. Phys. Chem.* **1968**, *72*, 108.
(18) Breshears, W. D.; Bird, F. *J. Chem. Phys.* **1978**, *68*, 2996.
(19) MacFadden, K. 0.; Tsckuikow-Roux, E. *J. Phys. Chem.* **1973**, *77*, 1475.
(20) Chase, M. W. *J. Phys. Chem. Ref. Data, Monogr.* **1998**, No. 9.
(21) Bettendorff, M.; Peyerimhoff, S. D. *Chem. Phys.* **1985**, *99*, 55.
(22) Radzig, A. A.; Smirnov, B. M. *Reference Data on Atoms, Molecules and Ions*; Springer-Verlag: Berlin, 1985.
(23) Herzberg, G. *Molecular Spectra and Molecular Structure I, Spectra of Diatomic Molecules*, 2nd ed.; Van Nostrand Reinhold Company: New York; 1950; Vol. 1.
(24) Barreto, P. R. P.; Vilela, A. F. A.; Gargano, R. *Int. J. Quantum Chem.* **2005**, *103*, 659.
(25) Harmony, M. D.; Myers, R. J. *J. Chem. Phys.* **1962**, *37*, 636.
(26) Ford, T. A.; Steele, D. *J. Phys. Chem.* **1996**, *100*, 19336.
(27) *CRC Handbook of Chemistry and Physics*; West, R. C., Astle, M. J., Beyer, W. H., Eds.; CRC Press: Boca Raton, FL, 1985.
(28) Lascola, R.; Withnall, R.; Andrews, L. *J. Phys. Chem.* **1998**, *92*, 2145.
(29) Gurvich, L. V.; Veyts, I. V.; Alcock, C. B. *Thermodynamic Properties of Individual Substances*, 4th ed.; Hemisphere Pub. Co.: New York, 1989.
(30) Berkowitz, J.; Greene, J. P.; Foropoulos, J., Jr.; Neskovic, O. M. *J. Chem. Phys.* **1984**, *81*, 6166.
(31) Shamasundar, K. R.; Arunan, E. *J. Phys. Chem. A* **2001**, *105*, 8533.
(32) Curtiss, L. A.; Raghavachari, K.; Redfern, P. C.; Rassolov, V.; Pople, J. A. *J. Chem. Phys.* **1997**, *106*, 1063.
(33) Aschi, M.; Grandinetti, F. *J. Mol. Struct.: THEOCHEM* **2000**, *497*, 205.
(34) Melius, C. F.; Ho, P. *J. Phys. Chem.* **1998**, *95*, 1410.
(35) Ricca, A. *Chem. Phys. Lett.* **1998**, *294*, 454.
(36) Curtiss, L. A.; Raghavachari, K.; Redfern, P. C.; Rassolov, V.; Pople, J. A. *J. Chem. Phys.* **1998**, *109*, 7764.
(37) Curtiss, L. A.; Raghavachari, K.; Redfern, P. C.; Rassolov, V.; Pople, J. A. *J. Chem. Phys.* **1999**, *110*, 4703.
(38) Truhlar, D. G.; Isaacson, A. D.; Garrett, B. C. In *Theory of Chemical Reaction Dynamics*; Baer, M. C., Ed.; CRC Press: Boca Raton, FL; 1985; Vol. 4.

JP903221B